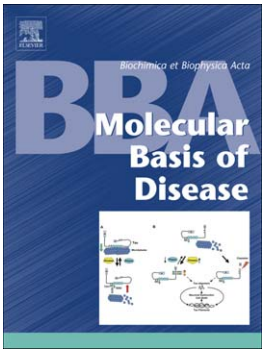

Spastin regulates VAMP7-containing vesicles trafficking in cortical neurons

C. Plaud, V. Joshi, M. Marinello, D. Pastré, T. Galli, P.A. Curmi, A. Burgo

PII: S0925-4439(17)30119-9
DOI: doi:10.1016/j.bbadis.2017.04.007
Reference: BBADIS 64738

To appear in: *BBA - Molecular Basis of Disease*

Received date: 13 December 2016
Revised date: 4 April 2017
Accepted date: 6 April 2017

Please cite this article as: C. Plaud, V. Joshi, M. Marinello, D. Pastré, T. Galli, P.A. Curmi, A. Burgo, Spastin regulates VAMP7-containing vesicles trafficking in cortical neurons, *BBA - Molecular Basis of Disease* (2017), doi:10.1016/j.bbadis.2017.04.007

Spastin regulates VAMP7-containing vesicles trafficking in cortical neurons

Plaud C.[1*], Joshi V.[1*], Marinello M.[1], Pastré D.[1], Galli T.[2], Curmi PA.[1] and Burgo A.[1]

[1]*Structure and Activity of Normal and Pathological Biomolecules, INSERM U1204, Université d' Evry, France.*

[2]*Inserm URL U950, Institut Jacques Monod, France.*

** These authors equally contribute to this work*

Corresponding author: andrea.burgo@univ-evry.fr

ABSTRACT

Alteration of axonal transport has emerged as a common precipitating factor in several neurodegenerative disorders including Human Spastic Paraplegia (HSP). Mutations of the *SPAST* (*SPG4*) gene coding for the spastin protein account for 40% of all autosomal dominant uncomplicated HSP. By cleaving microtubules, spastin regulates several cellular processes depending on microtubule dynamics including intracellular membrane trafficking. Axonal transport is fundamental for the viability of motor neurons which often have very long axons and thus require efficient communication between the cell body and its periphery. Here we found that the anterograde velocity of VAMP7 vesicles, but not that of VAMP2, two vesicular-SNARE proteins implicated in neuronal development, is enhanced in SPG4-KO neurons. We showed that this effect is associated with a slight increase of the level of acetylated tubulin in SPG4-KO neurons and correlates with an enhanced activity of kinesin-1 motors. Interestingly, we demonstrated that an artificial increase of acetylated tubulin by drugs reproduces the effect of Spastin KO on VAMP7 axonal dynamics but also increased its retrograde velocity. Finally, we investigated the effect of microtubule targeting agents which rescue axonal swellings, on VAMP7 and microtubule dynamics. Our results suggest that microtubule stabilizing agents, such as taxol, may prevent the morphological defects

observed in SPG4-KO neurons no simply rescuing the altered anterograde transport to basal levels but rather by increasing the retrograde velocity of axonal cargoes.

1. INTRODUCTION

Hereditary spastic paraplegias (HSPs) constitute a group of heterogeneous inherited diseases characterized by a progressive degeneration of the corticospinal tract axons and *fasciculus gracilis fibers* [1]. HSPs have a prevalence of 1-5:100 000 in most populations [2], and to date more than 70 loci and 59 genes (spastic paraplegia genes, SPG) have been identified in HSP patients. Progressive lower limb spasticity and weakness are the predominant but not the only characteristics of this group of neurological syndrome [3]. Only symptomatic treatments partially improving spasticity are available for HSP patients, and no preventive or curative measures are yet available [4].

Mutations in the *SPAST* (SPG4 in mice) gene, encoding spastin, account for approximately 40% of the familial and 20% of the sporadic cases within autosomal dominant HSP [5, 6]. Spastin is a member of the ATPases Associated with diverse cellular Activities (AAA) protein family [7, 8] involved in microtubule severing through an ATP-dependent mechanism [9, 10]. By breaking long microtubules into shorter fragments, spastin regulates microtubule dynamics [11-14] and its activity has been implicated in the control of different microtubule-dependent cellular processes including axonal transport, endosomal recycling, cytokinesis and ER shaping (Reviewed in [8,

15]). In neurons, spastin is involved in axonal branching [16] and regeneration [17], synaptic bouton formation [18], neurotransmission [19] and axonal growth receptor-mediated BMP signaling [20]. Studies in *SPAST*/SPG4 defective neuronal model demonstrated that a reduced expression of spastin may be associated with a lower number of dynamic microtubules [12-14] and an increases of the level of acetylated α-tubulin [21, 22], a posttranslational modification (PTM) of tubulin generally associated with stable microtubules [23, 24]. Axonal membrane traffic is also affected with a decreased and imbalanced motility of axonal cargoes, mainly mitochondria, but not of their velocities [22, 25, 26]. Axonal swelling, the prominent axonal abnormality observed in different *SPAST/SPG4* neuronal models and in *SPAST* human patients [22, 25-27], has been linked to microtubule dynamics and axonal transport defects. This was based on the fact that different organelles are found enriched in these structures [12, 25, 27] in particular disorganized microtubule network [12, 26] and on the observation that microtubule-targeting agents (MTA), such as taxol, vinblastine and nocodazole, at low concentration prevent/rescue such axonal swellings [12, 21, 22].

Data published up to now suggested that spastin regulates the axonal transport of mitochondria but little is known about the role of this protein in other axonal compartment implicated in the delivery and recycling of

membrane, lipids and other cytoplasmic material critical for neuronal development and integrity. The vesicular (v-) Soluble N-ethylmaleimide sensitive factor Attachment Receptors (SNARE) through the interaction with their target (t-) SNAREs, form the so-called trans-SNARE complex which mediates the final step of fusion between two membranes, a process needed for all of biology, from cell division to synaptic transmission [28, 29]. Between them, VAMP7 (also called TI-VAMP), is a ubiquitous v-SNARE involved in numerous cellular functions including mitosis, autophagy and membrane homeostasis (for reviews see [30, 31]). In neurons, VAMP7 was shown to localize in axons and dendrites and concentrate in the growth cone and has an important role in axonogenesis [32], neurite growth [33-35], pathfinding [36] and it may later be involved in neurotransmitter release [37, 38] and higher brain function [39]. Interestingly, the traffic of VAMP7 vesicles has been related to the molecular motor kinesin1 Kif5A [40] and to the cell-cell adhesion molecule L1-CAM [35] two genes linked to HSP, SPG10 [41] and SPG1 [42] respectively. Particularly, the interaction with Kif5A allows VAMP7 positive secretory vesicles formed in the somatic Golgi-apparatus to move along microtubule tracks out of the cell body towards the terminal [40].

Here we demonstrated that the anterograde velocity of VAMP7 containing vesicles is enhanced in cortical neurons derived from SPG4-KO mice. This

correlates with a significant increase of the level of acetylated tubulin but no other PTMs of tubulin and is also observed when neuronal cells were treated with drugs that induce an increase of acetylated tubulin. These results suggest that the lack or impairment of spastin expression induces a moderate increased level of acetylated tubulin which enhances the activity of molecular motors of kinesin-1 family and the consequent anterograde velocity of axonal cargoes such as VAMP7 vesicles. Finally, we analyzed the effects of MTA, such as taxol and nocodazole which prevent axonal swellings in SPG4-KO neurons, on microtubule dynamics and membrane traffic. The results support the fact that the rescue of a normal phenotype is not simply due to the restoration of the anterograde transport to basal levels.

2. MATERIALS AND METHODS

2.1 Antibodies

Mouse monoclonal Ab (mAb) anti-acetylated tubulin (clone6-11B-1) and anti-GAPDH were from Sigma-Aldrich. Mouse mAb anti-KIF5B (KN-01), rabbit polyclonal antibody (pAb) anti-detyrosinated tubulin and rat mAb anti-tyrosinated tubulin (YL 1/2) were from Millipore. Rabbit pAb anti-Polyglutamate

chain (polyE) was from Adipogen. Mouse mAb anti-EB1 was from BD Bioscience. Mouse mAb anti β-III tubulin (TUJ1) was from Covance. Mouse mAb anti-spastin (Sp 3G11/1), mouse mAb anti-katanin p60 and goat pAb anti-TAU (C-17) were from Santa Cruz. Rabbit polyclonal anti-stathmin was a kind gift from André Sobel (INSERM, Paris, France). Mouse mAb anti-β-tubulin was produced from the ATCC E7 hybridoma clone. Secondary antibodies for immunofluorescence Alexa Fluor 488- or 594-conjugated goat anti-rabbit, anti-mouse, anti-rat or donkey anti-goat were from Molecular Probes (Carlsbad, CA). Secondary antibodies for immunoblot IRDye 800CW or IRDye 680CW conjugated goat anti-rabbit, anti-mouse or anti-rat were from LI-COR Bioscience (Lincoln, Nebraska, USA).

2.2 cDNA, reagents and drug treatments

mRFP-VAMP7 and GFP-VAMP2 was previously described [43, 44]. EB3-GFP was previously described [12]. Mitotracker orange CM-H2 TMROS was from Molecular Probes (Invitrogen). Paclitaxel (Taxol; Sigma-Aldrich), Nocodazole (Sigma-Aldrich) or Trichostatin A (TSA; Tocris) were added to culture medium at the different final concentrations. Taxol and nocodazole were incubated for 14-16 h whereas TSA for 4 h at 37°C in 5% CO_2 and maintained during the

time-lapse imaging experiment. Drugs were kept as stock solution in DMSO and working dilution were prepared freshly at each day of the experiment. When transfected, neurons were treated with drugs after sufficient rest once the Lipofectamine-containing medium was replaced.

2.3 Primary culture of cortical neurons and genotyping

Primary culture of cortical neurons was prepared from embryonic mice (E17) as described previously [45]. Briefly brains were dissected in HBSS with Hepes (Invitrogen) and incubated with 0.25% trypsin (Invitrogen) for 15 min at 37°C. Cells were than dissociated through a fire-constricted Pasteur pipette in presence of DNase (0.1 mg/mL; Sigma-Adrich). Neurons were plated on poly-DL-ornithine-coated (Sigma-Aldrich) glass coverslips or petri dishes at the density of 25 000-50 000, 500000 or 4 000 000 cells respectively for 12-mm, 30-mm and 100-mm coverslip/dish in minimal essential medium (Gibco, Invitrogen) supplemented with 10% horse serum, 0.6% glucose, 2 mM glutamine, and 10 IU/mL penicillin–streptomycin. Embryo genotypes (Fig. S1) were identified during the preparation of culture using the KAPA Mouse Genotyping Kit (Kapabiosystems, Boston, USA). Sp^{+} and Sp^{Δ} alleles were detected by PCR using the primers *spin7F* or *spin 4F* and *spin7R* as described previously [27]. Neurons were grown and maintained in Neurobasal medium

without phenol red (Invitrogen), supplemented with 2% B27 and 2 mM L-glutamax (Invitrogen) for 4 to 7 days and then processed for analysis.

2.4 Immunofluorescence and integrated fluorescence analysis.

For PTMs of tubulin analyses, cortical neurons were fixed with 4% PFA-sucrose for 20 min at RT while for EB1 staining, neurons were fixed with methanol for 5 min at -20°C followed by 4% PFA-sucrose and then processed for immunofluorescence. For PTMs tubulin ratio analyses, the integrated fluorescence intensity was measured after background subtraction for each PTM from the cell body to the growth-cone of the axons by using the Metamorph software (Roper Scientific, Evry, France). The number of axons analyzed for the ratio of acetylated versus tyrosinated tubulin range from 40 to 140 depending on the experimental condition. Data were normalized to the acetylated/tyrosinated ratio of $Sp^{+/+}$ untreated cortical neurons cultured the same experimental day. For the ratio of detyrosinated versus tyrosinated tubulin a minimum of 20 axons were considered. Each experiment was repeated at least 3 times. Statistical significance was determined by using the GraphPad PRISM software.

2.5 Immunoblot assays and densitometry analysis

Neurons were lysed at 7-DIV in TSE (50 mM TrisHCl pH 8.0, 150 mM NaCl, 1 mM EDTA) added of 1% Triton x100 and protease inhibitors cocktail (Complete ULTRA Tablets, EDTA-Free, Roche) on ice. Between 4 and 10 μg of lysates for PTMs of tubulin analysis and 25 μg for other proteins were separated by SDS-PAGE by using 10 % acrylamide gels and then the proteins were transferred onto nitrocellulose membrane (Amersham Protran, GE Healthcare Life Sciences). After incubation in 5% nonfat dry milk in Tris-buffered saline containing Tween (TBS-T; 200 mM Tris, 0.15 M NaCl (TBS), 0.1% Tween 20, pH 7.3) membranes were incubated with specific primary antibodies overnight. After washing in TBS-T, the membranes were blotted with secondary antibodies (IR dye 680- or IR dye 800- conjugated). Detection was carried out by the Odyssey infrared imaging system (LI-COR Biosciences, Lincoln, NE, USA). For PTMs of tubulin studies, the integrated area of each band was quantified by densitometry analysis using the ImageJ software (Rasband, W.S., ImageJ, U. S. National Institutes of Health, Bethesda, MD, USA, http://imagej.nih.gov/ij/). The ratio of acetylated, tyrosinated or detyrosinated versus β-tubulin or tyrosinated tubulin as indicated in the figures was then calculated for each sample. Data were normalized to the

acetylated/tyrosinated or β-tubulin ratio value obtained from $Sp^{+/+}$ or $Sp^{\Delta/\Delta}$ untreated cortical neurons examined on the same experimental day.

2.6 Time-lapse imaging and tracking analysis

Neurons were transfected between 4-DIV and 6-DIV by using 1.5 μg of selected cDNA and 3 μL of Lipofectamine2000 (Life technologies) according to manufacturer's instructions. Medium was replaced after 3h by astrocyte-conditioned Neurobasal completed medium to reduce the toxicity of Lipofectamine2000. After sufficient resting, neurons were treated or not with drugs as described above. Time-lapse experiments were performed between 16-24 h after transfection using an inverted microscope Nikon Eclipse Ti equipped with Intensilight C-HGFI fiber source, a 60x/1.4 NA Plan-Apochromat oil-immersion Nikon objective, a 1.6x tube lens and a Neo-sCMOS digital camera (ANDOR, Belfast, Northern Ireland). Neurons were imaged every 1 sec over a time period of 3 min for FP tagged-v-SNARE vesicles or EGFP-EB3 and every 5 sec over a time period of minimum 5 min for Mitotracker Orange. Imaging was conducted in modified Krebs-Ringer-HEPES buffer (135 mM NaCl, 2.5 mM KCl, 1.2 mM MgCl, 2 mM $CaCl_2$, 20 mM HEPES, 11.1 mM glucose and pH 7.4). Temperature was controlled by warmed air (37°C). The power source and exposure time were the lowest possible to avoid

phototoxicity. FP tagged-v-SNARE vesicles, microtubule plus-ends or mitotracker were tracked within the proximal region of the longest neurite (i.e. the axon) for an average length of 100 μm by kymograph plugins of the Metamorph software (Roper Scientific). Speed and direction of v-SNARE vesicles, mitochondria and microtubule plus-ends were quantified by measuring the slope of the projection of the maximum intensity of fluorescence over the time obtained by kymograph while their number was measured manually. Run length of the individual moving object was calculated by measuring its displacement (over 5 μm) between two pauses. Selected videos were also analyzed with the Manual Tracking plugin, available on the ImageJ website (http://rsb.info.nih.gov/ij/plugins/track/track.html). Data were collected from 3 to 8 different neuronal cultures obtained from different $Sp^{+/+}$ or $Sp^{\Delta/\Delta}$ embryos. Number of neurons analyzed (N) and number of object tracked (n) are indicated in the figures. Statistical significance was determined by using GraphPad PRISM software.

3. RESULTS

To study the role of spastin in microtubule dynamics and axonal membrane traffic, we used cortical neurons from homozygous SPG4 mice ($Sp^{\Delta/\Delta}$; fig.S1 for characterization) which show strong pathological phenotype compared to

heterozygous mice [12, 27]. Neurons were cultured between 5 and 7 days in vitro (DIV), thus after the onset of axonal swelling [27].

3.1 Tubulin acetylation is increased in SPG4-KO neurons

We first analyzed whether or not the levels of PTMs of tubulin, particularly acetylation, were modified in the present SPG4 mutant neuronal model. As shown in figure 1A, western blot analysis showed that the levels of acetylated tubulin were slightly increased in 7-DIV $Sp^{\Delta/\Delta}$ neurons compared to control neurons ($Sp^{+/+}$) whereas the levels of total β-tubulin or that of tyrosinated tubulin, a marker of dynamic microtubules, were not significant affected (see also Figs. S2A-B). To evaluate and quantify the degree of tubulin acetylation observed in $Sp^{\Delta/\Delta}$ neurons, we treated $Sp^{+/+}$ neurons with the deacetylase inhibitor trichostatin A (TSA) which increases the level of acetylated tubulin in neurons (Fig. 1B) [46-48] and measured the ratio of both acetylated versus β-tubulin and tyrosinated tubulin by western blotting. The acetylated/β-tubulin ratio was increased by 22.4±2.3% in $Sp^{\Delta/\Delta}$ compared to $Sp^{+/+}$ neurons and by 39.4±6.9% and 38±1.4% in $Sp^{+/+}$ neurons treated with 100 nM or 500 nM TSA respectively (Fig. 1C). Similarly, the acetylated/tyrosinated ratio was increased by 20.1±3.2% in $Sp^{\Delta/\Delta}$ compared to $Sp^{+/+}$ neurons and by 42.3±7.2% and

50.7±13.7% in $Sp^{+/+}$ neurons treated with 100 nM or 500 nM TSA (Fig. 1D). To confirm the results obtained by WB, we quantified the integrated intensity of acetylated versus tyrosinated tubulin staining within the axons (Fig. 1E-F). Strikingly, we observed a similar and significant increase of this index by 27.0±5 % in $Sp^{\Delta/\Delta}$ neurons compared to control. On the other hand, TSA induced an increase of 44.0±12 % and 60±9 % respectively at 100 nM and 500 nM. We next investigated the effects of $Sp^{\Delta/\Delta}$ on others PTMs of tubulin known to be associated with stable microtubules such as detyrosination and polyglutamylation. We did not observe any significant changes in the levels of these PTMs in $Sp^{\Delta/\Delta}$ neurons (Fig. S2) confirming previous results [26, 27]. Particularly, the detyrosinated to tyrosinated tubulin ratio appeared similar in $Sp^{\Delta/\Delta}$ and control neurons. Finally, we found no effect of the lack of spastin on the expression level of proteins implicated in the dynamic of the microtubule network such as p60 katanin and stathmin, which were found altered in other spastin mutated cell models [26, 49] or of other proteins such as the molecular motor Kif5B and β-tubulin isotype III both implicated in the regulation of microtubule dynamics [50, 51] (Fig. S3).

Taken together these results demonstrate a specific imbalanced regulation of the extent of tubulin acetylation likely associated with an increase of microtubule stability within the axon in $Sp^{\Delta/\Delta}$ neurons.

3.2 The anterograde velocity of VAMP7, but not that of VAMP2, -containing vesicles is increased in SPG4-KO neurons

Increased acetylation levels of α-tubulin have been reported to enhance the recruitment and motility of the molecular motors of both the kinesin-1 subfamily and dynein which drive cargoes along the microtubule networks respectively in anterograde and retrograde direction [46, 52-54]. In order to explore the role of spastin on axonal transport we analyzed the motility of two similar but distinct membrane compartments identified by the v-SNAREs, VAMP7 and VAMP2 [55]. Unlike VAMP7, VAMP2 (also named Syb2), the main v-SNARE of mature synaptic vesicles, does not seem to be directly involved in axonal extension [56, 57] and it is also transported into the growth cones in neurons [58]. Interesting, VAMP7 and VAMP2 vesicles seem to be driven by two different families of kinesin motors, respectively the kinesin-1 Kif5A [40] and the kinesin-3 Kif1A [59]. We also analyzed the axonal transport of mitochondria which velocities are not altered in other SPG4-HSP neuronal models.

The dynamics of VAMP7 or VAMP2 vesicles were followed live in cortical neurons after transfection of respectively RFP-tagged VAMP7 (Fig. 2A

and movie S1) and GFP-tagged VAMP2 (Fig. 3A and movie S2), as previously described [40, 43, 44]. The mean (kymograph analysis) or the maximum (manual tracking, not shown) anterograde and retrograde velocities were then measured within the axon.

Quantification of VAMP7-vesicles velocities showed that in $Sp^{\Delta/\Delta}$ neurons, the anterograde speed was significantly higher than in $Sp^{+/+}$neurons (Fig. 2B and table 1) whereas the retrograde velocity of such vesicles was not affected (Fig. 2C). In order to investigate whether higher level of acetylated tubulin may by itself enhance the anterograde motility of VAMP7-positive vesicles, we treated $Sp^{+/+}$ and $Sp^{\Delta/\Delta}$ neurons with 500 nM TSA as described above. Interestingly, we found an increased VAMP7 anterograde velocity in TSA-treated $Sp^{+/+}$ neurons (Fig. 2B) similar to what we observed in the absence of spastin (0.99±0.04 μm/s and 0.95±0.05 μm/s respectively for untreated $Sp^{\Delta/\Delta}$ and TSA treated $Sp^{+/+}$ neurons, see also table 1). Even though TSA induces an increase of the acetylated to tyrosinated tubulin ratio higher than what is observed in $Sp^{\Delta/\Delta}$ neurons (2 fold, Fig. 1), this did not result in an additive effect on VAMP7 anterograde speed in $Sp^{\Delta/\Delta}$ neurons (0.91±0.07 μm/s for $Sp^{\Delta/\Delta}$ neurons treated with 500 nM TSA). On the other hand, TSA enhanced retrograde velocity of VAMP7-vesicles (Fig. 2C) compared to $Sp^{+/+}$

and $Sp^{\Delta/\Delta}$ untreated neurons (0.63±0.02 μm/s, 0.65±0.02 μm/s for $Sp^{+/+}$ and $Sp^{\Delta/\Delta}$ untreated neurons and 0.75±0.02 μm/s, 0.71±0.03 μm/s for $Sp^{+/+}$ and $Sp^{\Delta/\Delta}$ neurons treated with 500 nM TSA, see also table 1). The mean run length (up to 5 μm, measured between two pauses) of anterograde, but not retrograde, VAMP7 vesicles was also increased in $Sp^{\Delta/\Delta}$ neurons and TSA affected this parameter in a similar way as what it does for velocities (Fig. 2D). Finally, we did not find any significant difference in directionality (anterograde versus retrograde) of VAMP7 vesicles between control and $Sp^{\Delta/\Delta}$ neurons both untreated or treated with TSA (Fig. 2E).

On the contrary both the anterograde and retrograde velocity of VAMP2 containing vesicles (Fig. 3 and movie S2) were not altered in $Sp^{\Delta/\Delta}$ neurons compare to control neurons (anterograde, 0.42±0.03 μm/s vs 0.4±0.04 μm/s and retrograde, 0.39±0.02 μm/s vs 0.43±0.03 μm/s, respectively in control and $Sp^{\Delta/\Delta}$ neurons). TSA treatment did not upregulate their anterograde velocity (Fig. 3B; 0.42±0.03 μm/s and 0.38±0.03 μm/s, respectively in control and $Sp^{\Delta/\Delta}$ TSA-treated neurons) but again induces a significant increase of their retrograde velocity (Fig. 3C; 0.5±0.04 μm/s and 0.51±0.03 μm/s, respectively in control and $Sp^{\Delta/\Delta}$ TSA-treated neurons) similar to what observed for VAMP7 vesicles. Both the lack of spastin activity and TSA treatment did not influence

significantly the proportion of VAMP2 vesicles moving in anterograde or retrograde direction (Fig. 3D).

Finally we analyzed mitochondrial traffic by tracking mitochondria labelled with Mitotracker in $Sp^{+/+}$ and $Sp^{\Delta/\Delta}$ neurons (Fig. S4A and movie S3). Mitochondria mean velocities (excluding pauses) were not significantly different in $Sp^{+/+}$ and $Sp^{\Delta/\Delta}$ neurons treated or not with TSA (Fig. S4B-C). We did not observe differences in the total amount of actively transported mitochondria between $Sp^{\Delta/\Delta}$ and control neurons but we measured an imbalance, even though not significant, between anterograde and retrograde transport events in neurons (Fig. S4D).

These data show that VAMP7 anterograde transport, but not that of VAMP2 vesicles, is enhanced in a similar manner by SPG4-KO and TSA. In addition, TSA treatment induces an increase of retrograde velocity of both VAMP7 and VAMP2 vesicles. Mitochondria velocities seemed not to be affected by both spastin depletion and low doses of TSA in agreement with previous reports [22, 25, 26, 60].

3.3 Effects of MTA on microtubule dynamics and VAMP7 membrane traffic in $Sp^{\Delta/\Delta}$ cortical neurons.

Axonal swelling is the main histological hallmark of *SPAST*-HSP [21, 22, 27]. This morphological feature is likely caused by a deregulation of fast axonal transport [61-63]. Interestingly, MTA such as taxol and nocodazole at nanomolar concentration prevent/rescue axonal swelling in neurons from $Sp^{\Delta/\Delta}$ mice [12]. In order to investigate whether the MTA-dependent recovery of the normal phenotype of $Sp^{\Delta/\Delta}$ neurons may be related to a modification of VAMP7 vesicles' traffic, we treated neurons with taxol or nocodazole at doses previously shown to rescue the pathological phenotype in $Sp^{\Delta/\Delta}$ neurons [12].

3.3.1 MTAs affect similarly the morphology and the PTMs of tubulin in $Sp^{\Delta/\Delta}$ and control neurons.

Although, when used at substoichiometric concentrations these drugs alter the dynamic instability of microtubules without a significant impact on microtubule mass [64-66], different studies in isolated neurons demonstrated that they induce significant changes at the morphological level [47, 48] and on PTMs of

tubulin, including acetylation [47, 48, 67]. Thus, we first analyzed whether these drugs affect in different manner these features in $Sp^{\Delta/\Delta}$ and control neurons. As shown in figure 4A we confirmed that 10 nM taxol and 100 nM nocodazole drastically reduced the number of active microtubule plus-ends both in $Sp^{\Delta/\Delta}$ and control neurons (not shown) in agreement with a reduction of microtubule dynamics. Nocodazole completely abolished the active microtubule plus-end [68, 69] while after taxol treatment they appeared less abundant, shorter and tend to accumulate in the distal part of neurites [48, 70]. Live imaging analysis of EB3-GFP, a plus-end marker of microtubule [68], in $Sp^{+/+}$ and $Sp^{\Delta/\Delta}$ neurons treated or not with the drugs confirmed that taxol did not completely abolish active microtubule plus-ends (Fig. S5 and movie S4). Quantification of the speed of EB3-GFP comets along the axon did not reveal differences in the polymerization rate in $Sp^{+/+}$ and $Sp^{\Delta/\Delta}$ neurons treated or not with taxol [12, 70] (Fig. S5B). Confirming immunofluorescence experiments, EB3 lifetime was reduced by taxol treatment (Fig. S5C). Then we showed (Fig. 4B-C) that most taxol-treated (10 nM) neurons have straighter long neurites characterized by fewer branches [48] whereas nocodazole-treated neurons (100 nM) developed just one or two long processes with a strong reduction of minor neurites [48] associated with an important disorganization of the microtubule network particularly revealed by tyrosinated tubulin staining. The effects of taxol and nocodazole are dose-dependent (Figs. S6 and S7). Finally

we analyzed the effects of these drugs on the level of PTMs of tubulin. As expected, taxol-treated neurons showed high ratio of acetylated versus tyrosinated microtubules within the axon both in $Sp^{+/+}$ and $Sp^{\Delta/\Delta}$ neurons (Fig. 4D). Interestingly, this index was also significantly increased in nocodazole-treated neurons. WB analysis (Fig. 4E-G) revealed that taxol significantly increased acetylated tubulin (by 32.3±8.3% and 15.5±4.4% in taxol-treated $Sp^{+/+}$ and $Sp^{\Delta/\Delta}$ neurons respectively; Fig. 4G) and strongly reduced the amount of tyrosinated tubulin [71] which resulted in a high acetylated to tyrosinated tubulin ratio. Nocodazole-treated neurons showed also an increase of this index likely due to the depolymerization of the dynamic-tyrosinated microtubules. In agreement with previous observations the microtubule mass was not altered by these drugs (Fig. 4E, β-tubulin).

These results demonstrate that the effects of taxol or nocodazole on microtubule dynamics, neuronal morphology and the level of PTMs of tubulin are not significant different between control and $Sp^{\Delta/\Delta}$ neurons.

3.3.2 MTA did not restore altered VAMP7 anterograde speed to basal level.

We then examined whether these drugs alter the transport of VAMP7 vesicles in $Sp^{\Delta/\Delta}$ and control neurons. Taxol significantly increased the anterograde mean speed of VAMP7 vesicles in $Sp^{+/+}$ neurons up to a level close to what is measured in untreated $Sp^{\Delta/\Delta}$ neurons but it did not modify this velocity when added in $Sp^{\Delta/\Delta}$ neurons (Fig. 5A and table 1). On the other hand, taxol increased the VAMP7 retrograde mean speed both in $Sp^{+/+}$ and $Sp^{\Delta/\Delta}$ neurons (0.83±0.04 μm/s versus 0.79±0.03 μm/s for $Sp^{+/+}$ and $Sp^{\Delta/\Delta}$ neurons respectively; Fig. 5B and table 1). On the contrary, nocodazole did not affect VAMP7 anterograde or retrograde velocities. Run length showed a similar profile than velocities with the exception of taxol treatment which did not increase this parameter in $Sp^{+/+}$ neurons and reduced it in $Sp^{\Delta/\Delta}$ neurons (Figs. 5C-D). Again, these drugs did not modify the proportion of VAMP7 vesicles moving in anterograde or retrograde direction (Fig. 5E and see also Fig. 2E).

Taken together these data suggest that nocodazole and taxol did not restore the altered anterograde axonal transport of VAMP7 vesicles observed in $Sp^{\Delta/\Delta}$ cortical neurons. However taxol increases VAMP7 retrograde velocity similar to TSA treatment.

4. DISCUSSION

Despite a documented implication of spastin in the regulation of microtubule dynamics, its role on microtubule-based membrane axonal transport is not well established so far. Moreover, previous studies in spastin deficient neuronal models failed to find any correlation between an increased level of acetylated tubulin, generally associated with a reduced activity of spastin, and the dynamics of axonal membrane cargoes.

4.1 The level of acetylated tubulin, but no that of other PTMs of tubulin, is increased in SPG4-KO neurons.

In the $Sp^{\Delta/\Delta}$ neuronal model used here, we showed that the acetylation level of tubulin was slightly but significant increased compared to control neurons in agreement with previous observation in others SPG4-HSP neuronal model [19, 21, 22]. This effect seems to be restricted to acetylation since we neither observe the alteration of others PTMs of tubulin such as tyrosination, de-tyrosination and polyglutamylation (Fig. S2) nor changing in the expression of others proteins implicated in microtubule dynamics (Fig. S3). Tarrade and coworkers suggested that de-tyrosinated tubulin is enriched in

axonal swelling but they did not observe a general increase of this PTM as in this work [27]. Thus, an increased level of acetylated tubulin may represent a specific response to a reduced or a lacked activity of spastin in neurons. Indeed, theoretically, a lower concentration of spastin results in longer microtubules which should be a better substrate for the slow catalytic activity of the α-tubulin acetyl transferase (TAT)[72, 73]. Given the importance of spastin in several neuronal processes such as branch formation [16], alternative molecular mechanisms can compensate for the lack of expression of this protein. Interesting, the activity of katanin, the other microtubules severing protein highly expressed in the CNS [74], is regulated by the acetylation state of microtubules [75]. Therefore the increased level of acetylation observed in $Sp^{\Delta/\Delta}$ cortical neurons may enhance the severing activity of katanin without necessarily requiring an increase in its expression (Fig. S3).

4.2 Selective regulation of the VAMP7 anterograde velocity in $Sp^{\Delta/\Delta}$ neurons.

It is worth noting that microtubule-dependent motor proteins show a higher affinity towards stable microtubules [47, 52, 76]. Particularly, an increased acetylation levels of α-tubulin enhances the motility and the

recruitment of both kinesin-1 and dynein to microtubules [46, 52-54] which is in line with an augmented vesicle transport on stable microtubules. Previous studies on the axonal transport of mitochondria demonstrated that only their motility was altered while the velocities were unchanged suggesting that the activity of the molecular motors was unaffected by a reduction of spastin activity [22, 25, 26]. Indeed, in the present $Sp^{\Delta/\Delta}$ neuronal model, we confirm that mitochondria velocities are unaffected (Fig. S4) but we found that the anterograde velocity of VAMP7 vesicles was significantly increased in agreement with an enhanced activity of kinesin motors. Due to the abovementioned effects of acetylation on motors, we think that this later effect likely depends on the increased level of acetylated tubulin observed in $Sp^{\Delta/\Delta}$ neurons. Low doses of drugs such as TSA and taxol which by different mechanisms increase the proportion of acetylated stable versus dynamic microtubules [46-48] enhance the anterograde velocity of VAMP7 vesicles to an extent similar to what was observed in $Sp^{\Delta/\Delta}$ neurons. This again fits well with an augmented activity of kinesin motors in both $Sp^{\Delta/\Delta}$ and drugs-treated neurons. On the contrary the anterograde velocity of vesicles containing the v-SNARE VAMP2 is unchanged in $Sp^{\Delta/\Delta}$ and TSA treated neurons, suggesting that only the transport of specific axonal cargoes is altered by a reduction of spastin activity. An easy explanation of these results is that VAMP7 and VAMP2 vesicles are likely travelled along microtubules by two different classes

of kinesin motors, respectively the kinesin-1 Kif5A [40] and the kinesin-3 Kif1A [59]. Indeed, only the members of kinesin-1 family associate preferentially with PTM-marked microtubules in cells, particularly acetylation, whereas kinesin-3 motors show no selectivity for PTM-marked tracks [53]. However, this conclusion is likely too simplistic since the transport of other axonal cargoes driven at least by a kinesin-1 motor such as mitochondria [77, 78] and APP vesicles [79, 80] are not affected in the same manner in spastin defective neurons [22, 25, 26]. Other parameters such as the size of the cargo, the number of motor engaged and probably the presence of specific adaptor proteins [81-83] may have an important role in the outcome of axonal cargo transport due to the SPG4 reduced activity.

4.3 Higher increase of tubulin acetylation enhances the activity of dynein motor.

In TSA-treated neurons we observed also an increase of the retrograde velocity of both VAMP7 and VAMP2 vesicles which suggest an increased activity of dynein motors. This effect correlates with the higher increase of tubulin acetylation induced by this drug compare to that observed in $Sp^{\Delta/\Delta}$ neurons (Fig. 1). TSA-induced tubulin acetylation has been already shown to

enhance the velocities both in anterograde and retrograde direction of the BDNF-containing vesicles in neurons [46]. In cells the mechanism by which the molecular motors are recruited and activated by tubulin acetylation is not fully understood. *In vitro* experiments [84, 85] suggest that additional *in vivo* mechanisms depending on tubulin acetylation, such as the binding to microtubules of specific MAPs [86] or structural changes that occur in the microtubule lattice, enhance the affinity of molecular motors for microtubules tracks and their motility. The most likely scenario is that the magnitude of tubulin acetylation may affect differently these or other unknown parameters and only higher level of tubulin acetylation significantly enhances the interaction and the activity of dynein motor and/or its adaptor proteins to microtubules.

4.4 Altered anterograde transport is not restored to basal level by MTA

Axonal swelling is a feature of a variety of motor neuron diseases in humans and other vertebrates [87, 88] including *SPAST*-HSP [21, 22, 27]. These pathological structures are likely caused by a deregulation of fast axonal transport and are often filled with several axonal cargos including vesicles, synaptic membrane proteins and mitochondria [61-63]. MTA hold

promise as potential therapeutic treatments for several neurodegenerative diseases [89, 90] and, interestingly, drugs such as taxol and nocodazole used at nanomolar concentration prevent/rescue axonal swelling in cortical neurons from $Sp^{\Delta/\Delta}$ mice [12]. However to date, the molecular and cellular mechanisms by which these drugs rescue the normal phenotype of $Sp^{\Delta/\Delta}$ neurons are not fully understood. In this work we show that taxol and nocodazole did not rescue the altered anterograde velocity of VAMP7-vesicles observed in $Sp^{\Delta/\Delta}$ neurons (Fig. 5). However, VAMP7 vesicles retrograde velocity was increased by taxol, but not nocodazole, in control and $Sp^{\Delta/\Delta}$ neurons, similarly to what observed with TSA (see table 1) and in correlation with the increased level of acetylated tubulin of taxol-treated neurons (Fig. 4D-G). Although a direct link between axonal swelling formation and perturbation of axonal traffic has not been clearly established so far, the present results suggest that MTA may rescue axonal swelling in SPG4-KO model not simply by returning the membrane traffic properties to basal level but rather that taxol, and likely other drugs that increase acetylated tubulin, may counterbalance the altered anterograde traffic by increasing the retrograde velocity of axonal cargoes, such it is the case for VAMP7 vesicles.

4.3 Conclusion

In conclusion, these and previous results are consistent with a model (Fig. 6) in which the absence or the reduced expression of spastin likely results in longer and locally disorganized microtubule arrays within the axons [12, 26]. This pathological condition leads to an increased level of acetylated tubulin which enhances, directly or indirectly, the anterograde speed of small axonal cargos driven by kinesin-1 motors such as VAMP7 vesicles. The consequent deregulation of axonal transport might induce axonal defect such as axonal swelling. Our results could not definitively state whether VAMP7 is directly involved in the SPG4-linked disease and this assumption likely requires further investigation. However, the fact that the dynamics of VAMP2 vesicles and mitochondria are not affected in SPG4-KO neurons strongly suggests that an altered transport of VAMP7-positive compartment may trigger the onset and/or progression of the SPG4-linked neurodegeneration. Indeed, a fine regulation of VAMP7 transport, whose role is pivotal to support plasma membrane expansion and remodeling during neuronal development [32, 33, 40], is surely needed to maintain the stability and viability of the longest neurons of the CNS.

Figure Legends

Figure 1. Acetylated tubulin is increased in $Sp^{\Delta/\Delta}$ neurons. A, Representative immunoblot analysis for acetylated, tyrosinated and β-tubulin performed on proteins extracted from five different $Sp^{+/+}$ and $Sp^{\Delta/\Delta}$ neuronal cultures at DIV7. Note that for acetylated and tyrosinated tubulin the signals come from the same area of the same membrane (overlay). **B**, Representative immunoblot of proteins from $Sp^{+/+}$ cultured neurons treated with 100 nM or 500 nM TSA for 4 h. Quantification of the acetylated / β-tubulin (**C**) and acetylated / tyrosinated tubulin ratio (**D**) based on the integrated fluorescence intensity of the respective WB bands and normalized for the value measured in control $Sp^{+/+}$ cells. Each point represents different embryos. **E**, $Sp^{\Delta/\Delta}$ and $Sp^{+/+}$ cortical neurons at 4-DIV were fixed and co-labelled for acetylated and tyrosinated tubulin. $Sp^{+/+}$ cortical neurons were also treated with 100 nM (not shown) or 500 nM TSA for 4 h to reproduce the treatment applied for immunoblot analyses.**F**, Quantification of the acetylated / tyrosinated tubulin ratio within the axon. The integrated fluorescence intensity of the two PTMs of tubulin was measured within the longest neurite (i.e. axon) from cell body to the growth cone and the acetylated / tyrosinated tubulin ratio was calculated and normalized to the value obtained in $Sp^{+/+}$ untreated neurons. Data are shown

as mean ± SEM. Significance was determined by one-way ANOVA, Dunnett's posttest. *p<0.05, **p<0.01, ***p<0.005, ****p<0.001. ns, not significant. Scale bars, 20 μm.

Figure 2. The anterograde velocity of VAMP7-vesicles is increased in $Sp^{\Delta/\Delta}$ neurons. A, Cortical neurons derived from control ($Sp^{+/+}$) and spastin knock-out ($Sp^{\Delta/\Delta}$) mice were transfected at DIV4 with RFP-VAMP7. Neurons were also treated or not with 500 nM TSA for 4h. The dynamics of VAMP7-vesicles within the axon was analyzed 16 h after transfection and their speed and directionality were quantified by kymograph (**A**). Arrow dot lines indicate the regions analyzed to build the kymograph showed below the microphotograph and the orientation of the axon from the cell body to the periphery. **B-C**, Quantification of the anterograde and retrograde velocity of VAMP7-vesicles. **D,** Quantification VAMP7 vesicles anterograde and retrograde run length (distance between two pauses over 5 μm) in $Sp^{+/+}$ and $Sp^{\Delta/\Delta}$ untreated and TSA treated neurons. **E**, Proportion between VAMP7 transport events in the anterograde and retrograde direction. N and n, number of axons and VAMP7-vesicles respectively analyzed in the panels B-E. Data are shown as mean ± SEM. Significance is determined by one-way ANOVA, Dunnett's posttest. *p<0.05; **p<0.01; ***p<0.005; ns, not significant. Scale bars, 20 μm.

Figure 3. Spastin did not regulate the anterograde velocity of VAMP2 vesicles. A, Cortical neurons derived from control ($Sp^{+/+}$) and spastin knock-out ($Sp^{\Delta/\Delta}$) mice were transfected at DIV4 with GFP-VAMP2. Neurons were also treated or not with 500 nM TSA for 4h. The dynamics of VAMP2-vesicles within the axon was analyzed 16 h after transfection and their speed and directionality were quantified by kymograph (**A**). Arrow dot lines indicate the regions analyzed to build the kymograph showed below the microphotograph and the orientation of the axon from the cell body to the periphery. **B-C**, Quantification of the anterograde and retrograde velocity of VAMP2-vesicles. **D**, Proportion between VAMP2 transport events in the anterograde and retrograde direction. N and n, number of axons and VAMP2-vesicles respectively analyzed in the panels B-D. Data are shown as mean ± SEM. Significance is determined by one-way ANOVA, Dunnett's posttest. *$p<0.05$; ns, not significant. Scale bars, 20 μm.

Figure 4. Effect of MTA on microtubule dynamics, neuronal morphology and the levels of PTMs of tubulin in cortical neurons. A, $Sp^{\Delta/\Delta}$ cortical neurons were treated or not with 10 nM taxol or 100 nM Nocodazole for 14-16h, fixed and labelled for the microtubule plus-ends marker EB1(arrowheads). Nocodazole completely abolished the active microtubule plus-end while taxol did not. Control (**B**) and $Sp^{\Delta/\Delta}$ (**C**) cortical neurons were

treated or not with 10 nM taxol or 100 nM Nocodazole for 14-16h, fixed and stained for acetylated and tyrosinated tubulin. **D**, Quantification of the acetylated / tyrosinated tubulin ratio within the axon. The integrated fluorescence intensity of the two PTMs of tubulin was measured within the longest neurite (i.e. axon) from cell body to the growth cone and the acetylated / tyrosinated tubulin ratio was calculated and normalized to the value obtained in $Sp^{+/+}$ or $Sp^{\Delta/\Delta}$ untreated neurons. Data are shown as mean ± SEM. Significance was determined by one-way ANOVA, Dunnett's posttest. *p<0.05, **p<0.01, ****p<0.001. **E**, Representative Immunoblot of proteins from 7-DIV cultured neurons treated with the drugs. Quantification of the acetylated versus tyrosinated (**F**) or β-tubulin (**G**) ratio based on the integrated fluorescence intensity of the respective WB bands and normalized for the value measured in $Sp^{+/+}$ or $Sp^{\Delta/\Delta}$ untreated cells. Data are shown as mean ± SD. Scale bars, 20 μm.

Figure 5. Taxol increases retrograde velocity of VAMP7 vesicles in $Sp^{\Delta/\Delta}$ neurons.

$Sp^{+/+}$ and $Sp^{\Delta/\Delta}$ cortical neurons were transfected with RFP-VAMP7 and then treated or not with 10 nM taxol or 100 nM Nocodazole for 14-16h. Dynamics of moving VAMP7-vesicles within the axon was analyzed 16 h after transfection

and their speed and directionality were quantified by kymograph as shown in figure 2. **A-B**, Quantification of anterograde (**A**) or retrograde (**B**) velocity of VAMP7 moving vesicles within the axon treated or not with the drugs. **C,** Quantification of run length (distance between two pauses over 5 μm) of anterograde and retrograde moving VAMP7 vesicles in $Sp^{+/+}$ and $Sp^{\Delta/\Delta}$ untreated and drugs-treated neurons. **D**, Proportion of VAMP7 transport events in anterograde or retrograde direction in drugs treated neurons. N and n, number of axons and VAMP7-vesicles respectively analyzed in the panels A-E. Data are shown as mean ± SEM. Significance is determined by one-way ANOVA, Dunnett's posttest. **p<0.01; ***p<0.005;****p<0.001. ns, not significant.

Figure 6. A proposed model to account for spastin defects and tubulin acetylation in VAMP7 axonal transport.

By cleaving microtubules, spastin controls the mean length of microtubules. In pathological conditions, the lower level of functional spastin leads to a lower number of severing events and longer microtubules. This condition is associated with a weak increase of the level of acetylated tubulin which enhances the binding and the activity of the molecular motors of kinesin-1 family resulting in a selective increase of VAMP7 vesicles anterograde velocity. Higher level of tubulin acetylation, induced for example by MTA or

inhibitors of HDAC6, increases also retrograde velocity of VAMPs vesicles suggesting an augmented activity of dynein motors.

SUPPLEMENTARY INFORMATION

Supplementary Figure 1. Identification and characterization of SPG4 mutated embryos.

A, PCR amplification of the Sp^{+} and Sp^{Δ} alleles from DNA of $Sp^{+/+}$ (wild-type), $Sp^{\Delta/\Delta}$ (homozygous) and $Sp^{\Delta/+}$ (heterozygous) embryos using *spin 4F* or *spin7F* and *spin7R* primers [27]. Genotype reveals a band of 190 bp and 850 bp respectively for Sp^{+} and Sp^{Δ} alleles. M, ladder. **B**, Immunoblot analysis using the Sp 3G11/1 monoclonal antibody and protein extracts from cortical neurons in culture at 7-DIV obtained from different $Sp^{+/+}$ and $Sp^{\Delta/\Delta}$ embryos. WB shows a band of approximatively 60 kDa corresponding to the full-length spastin only in $Sp^{+/+}$ embryos.

Supplementary figure 2. The levels of detyrosinated and polyglutamylated tubulin are unchanged in $Sp^{\Delta/\Delta}$ neurons.

A, Representative immunoblot analysis for tyrosinated and total β-tubulin of lysate from different $Sp^{+/+}$ and $Sp^{\Delta/\Delta}$ neuronal cultures at 7-DIV. **B**, Quantification of the ratio between the integrated fluorescent intensity of the band for tyrosinated versus β-tubulin. **C**, Representative immunoblot analysis for detyrosinated and tyrosinated tubulin of proteins extracted from six different $Sp^{+/+}$ and $Sp^{\Delta/\Delta}$ neuronal cultures at 7-DIV. **D**, Measurement of the ratio between the integrated fluorescent intensity of the band for detyrosinated versus tyrosinated tubulin did not show difference in the level of these two PTMs of tubulin. **E,** $Sp^{+/+}$ and $Sp^{\Delta/\Delta}$ cortical neurons at 4-DIV were fixed and co-stained for detyrosinated and tyrosinated tubulin. **F**, The integrated fluorescence intensity was measured within the longest neurite (i.e. axon) from the cell body to growth cone. The ratio between the integrated intensity of detyrosinated and tyrosinated tubulin is not altered by the lack of spastin. **G**, Representative Immunoblot of polyglutamylated and tyrosinated tubulin in $Sp^{+/+}$ and $Sp^{\Delta/\Delta}$ neurons. Polyglutamylation is not modified in $Sp^{\Delta/\Delta}$ neurons. Data are shown as average ± SEM. Significance is determined by unpaired t-test student. ns, not significant. Scale bars, 20 μm.

Supplementary figure 3. Representative proteins implicated in microtubule dynamics are not dysregulated in $Sp^{\Delta/\Delta}$ neurons.

Immunoblot analysis for stathmin, p60 katanin, the molecular motors Kif5B and the β-tubulin isotype III in different $Sp^{+/+}$ (wild-type), $Sp^{\Delta/\Delta}$ (homozygous) and $Sp^{\Delta/+}$ (heterozygous) cortical neurons in culture at DIV7. The expression level of these proteins did not vary between the different spastin genotype. Perturbation of microtubule dynamics by treatment with 10 nM taxol or 100 nM Nocodazole for 16h did not alter their expression level.

Supplementary figure 4. Mitochondria velocities are not altered in $Sp^{\Delta/\Delta}$ neurons.

A, Cortical neurons derived from $Sp^{+/+}$ and $Sp^{\Delta/\Delta}$ mice were loaded with mitotracker orange and imaged live. Neurons were also treated or not with 500 nM TSA for 4h. Motility and speed of moving mitochondria were tracked by using kymograph analysis. **B**, Quantification of mitochondria velocity moving in anterograde direction ($Sp^{+/+}$ vs $Sp^{\Delta/\Delta}$ neurons: untreated, 0.18±0.02 μm/s vs 0.22±0.02 μm/s; TSA-treated, 0.20±0.02 μm/s vs 0.15±0.04 μm/s). **C**, Quantification of mitochondria velocity moving in retrograde direction ($Sp^{+/+}$ vs $Sp^{\Delta/\Delta}$ neurons: untreated, 0.28±0.02 μm/s vs 0.28±0.01 μm/s; TSA-treated, 0.26±0.02 μm/s vs 0.29±0.03 μm/s). **D**, Proportion of mitochondria events in

the anterograde or retrograde direction in $Sp^{+/+}$ and $Sp^{\Delta/\Delta}$ neurons. N and n, number of axons and mitochondria analyzed respectively showed in the panels B-D. Data are shown as mean ± SEM. Significance is determined by one-way ANOVA, Dunnett's posttest. *p<0.05; ns, not significant. Scale bars, 20 μm.

Supplementary figure 5. Dynamics of microtubule plus-end EB3 protein in $Sp^{+/+}$ and $Sp^{\Delta/\Delta}$ cortical neurons

A, $Sp^{+/+}$ and $Sp^{\Delta/\Delta}$ cortical neurons were transfected with EB3-GFP and treated or not with 10 nM taxol for 14-16h. EB3-GFP comets were tracked by time-lapse imaging within the axons and their speed and lifetime were measured by kymograph analysis. Quantification of velocity (**B**) and lifetime (**C**) of EB3-GFP comets in untreated or taxol treated neurons. Each point represents the average between 40 and 100 EB3-particles resulting from neuronal cultures of different embryos. Data are shown as mean ± SEM. Scale bars, 20 μm.

Supplementary figure 6. Neuronal morphological changes induced by taxol in $Sp^{\Delta/\Delta}$ neurons are concentration dependent.

Low density $Sp^{\Delta/\Delta}$ cortical neurons at 4-DIV were treated with 1, 10 or 100 nM taxol for 16h, fixed and co-labelled for acetylated and tyrosinated tubulin. The effects of taxol were detectable starting from the concentration of 10 nM. Scale bars, 20 μm.

Supplementary figure 7. Neuronal morphological changes induced by nocodazole are concentration dependent.

Low density $Sp^{\Delta/\Delta}$ (A) and $Sp^{+/+}$ (B) cortical neurons at 4-DIV were treated with 10 nM, 100 nM and 1 μM nocodazole for 16h, fixed and co-labelled for acetylated and tyrosinated tubulin. The effects of nocodazole were observable starting from the concentration of 100 nM. Only likely hyperacetylated microtubules were detectable in 1 μM nocodazole treatment. Morphological changes were not significant different between $Sp^{\Delta/\Delta}$ and $Sp^{+/+}$ neurons in all the tested conditions. Scale bars, 20 μm.

Supplementary movie 1. RFP-VAMP7 containing vesicles dynamics in $Sp^{+/+}$ (left) and $Sp^{\Delta/\Delta}$ (right) 5-DIV cortical neurons. Cortical neurons were transfected for 3h with RFP-VAMP7 at 4-DIV and imaged live 16h after transfection. Time is indicated in min:sec. Acceleration 5×. Scale bar, 20 μm.

Supplementary movie 2. GFP-VAMP2 containing vesicles dynamics in $Sp^{+/+}$ (left) and $Sp^{\Delta/\Delta}$ (right) 5-DIV cortical neurons. Cortical neurons were transfected for 3h with GFP-VAMP2 at 4-DIV and imaged live 16h after transfection. Time is indicated in min:sec. Acceleration 5×. Scale bar, 20 μm.

Supplementary movie 3. Dynamics of mitochondria in $Sp^{+/+}$ (left) and $Sp^{\Delta/\Delta}$ (right) 5-DIV cortical neurons. Cortical neurons were loaded with 100 mM Mitotracker orange (Invitrogen) for 15 min at 37°C, washed 2 times with recording medium and imaged live. Time is indicated in min:sec. Acceleration 24×. Scale bar, 20 μm.

Supplementary movie 4. Dynamics of EB3-GFP in untreated (left) and 10 nM taxol-treated (right) $Sp^{\Delta/\Delta}$ cortical neurons. Cortical neurons were transfected for 3h with EB3-GFP at 4-DIV. After sufficient resting time, neurons were

treated or not with 10 nM taxol for 16-18h and then imaged live. Time is indicated in min:sec. Acceleration 5×.

Acknowledgements

All data generated or analyzed during this study are included in this published article and its supplementary information files. We are grateful to Aurore Pignerol for performing some WB experiments. Animal experiments were performed according to the governmental guidelines n° 86/609/CEE. This work was funded by grants from INSERM, University of Evry and the Association Française contre les Myopathies (AFM; Research Programs n° 18813). CP was supported by DIM Cerveau et Pensée, Ile de France. The authors declare that they have no competing interests.

Authors' contributions

CP and MM performed some time lapse video imaging and WB experiments. VJ performed genotyping analysis and some WB experiments. AB performed and analyzed all the others experiments, interpreted the results and was the major contributor in writing the manuscript. VJ, DP, TG and PC participate to the writing and the critical reading of the manuscript. All authors read and approved the final manuscript.

REFERENCES

[1] G.C. Deluca, G.C. Ebers, M.M. Esiri, The extent of axonal loss in the long tracts in hereditary spastic paraplegia, Neuropathology and applied neurobiology, 30 (2004) 576-584.

[2] G. Novarino, A.G. Fenstermaker, M.S. Zaki, M. Hofree, J.L. Silhavy, A.D. Heiberg, M. Abdellateef, B. Rosti, E. Scott, L. Mansour, A. Masri, H. Kayserili, J.Y. Al-Aama, G.M. Abdel-Salam, A. Karminejad, M. Kara, B. Kara, B. Bozorgmehri, T. Ben-Omran, F. Mojahedi, I.G. Mahmoud, N. Bouslam, A. Bouhouche, A. Benomar, S. Hanein, L. Raymond, S. Forlani, M. Mascaro, L. Selim, N. Shehata, N. Al-Allawi, P.S. Bindu, M. Azam, M. Gunel, A. Caglayan, K. Bilguvar, A. Tolun, M.Y. Issa, J. Schroth, E.G. Spencer, R.O. Rosti, N. Akizu, K.K. Vaux, A. Johansen, A.A. Koh, H. Megahed, A. Durr, A. Brice, G. Stevanin, S.B. Gabriel, T. Ideker, J.G. Gleeson, Exome sequencing links corticospinal motor neuron disease to common neurodegenerative disorders, Science, 343 (2014) 506-511.

[3] J.K. Fink, Hereditary spastic paraplegia: clinico-pathologic features and emerging molecular mechanisms, Acta neuropathologica, 126 (2013) 307-328.

[4] C. Depienne, G. Stevanin, A. Brice, A. Durr, Hereditary spastic paraplegias: an update, Curr Opin Neurol, 20 (2007) 674-680.

[5] N. Fonknechten, D. Mavel, P. Byrne, C.S. Davoine, C. Cruaud, D. Bonsch, D. Samson, P. Coutinho, M. Hutchinson, P. McMonagle, J.M. Burgunder, A. Tartaglione, O. Heinzlef, I. Feki, T. Deufel, N. Parfrey, A. Brice, B. Fontaine, J.F. Prud'homme, J. Weissenbach, A. Durr, J. Hazan, Spectrum of SPG4 mutations in autosomal dominant spastic paraplegia, Human molecular genetics, 9 (2000) 637-644.

[6] J. Hazan, N. Fonknechten, D. Mavel, C. Paternotte, D. Samson, F. Artiguenave, C.S. Davoine, C. Cruaud, A. Durr, P. Wincker, P. Brottier, L. Cattolico, V. Barbe, J.M. Burgunder, J.F. Prud'homme, A. Brice, B. Fontaine, B. Heilig, J. Weissenbach, Spastin, a new AAA protein, is altered in the most frequent form of autosomal dominant spastic paraplegia, Nature genetics, 23 (1999) 296-303.

[7] J.M. Solowska, P.W. Baas, Hereditary spastic paraplegia SPG4: what is known and not known about the disease, Brain, 138 (2015) 2471-2484.

[8] C. Blackstone, C.J. O'Kane, E. Reid, Hereditary spastic paraplegias: membrane traffic and the motor pathway, Nature reviews, 12 (2011) 31-42.

[9] A. Roll-Mecak, R.D. Vale, The Drosophila homologue of the hereditary spastic paraplegia protein, spastin, severs and disassembles microtubules, Current biology : CB, 15 (2005) 650-655.

[10] A. Roll-Mecak, R.D. Vale, Structural basis of microtubule severing by the hereditary spastic paraplegia protein spastin, Nature, 451 (2008) 363-367.

[11] E. Riano, M. Martignoni, G. Mancuso, D. Cartelli, F. Crippa, I. Toldo, G. Siciliano, D. Di Bella, F. Taroni, M.T. Bassi, G. Cappelletti, E.I. Rugarli, Pleiotropic effects of spastin on neurite growth depending on expression levels, Journal of neurochemistry, 108 (2009) 1277-1288.

[12] C. Fassier, A. Tarrade, L. Peris, S. Courageot, P. Mailly, C. Dalard, S. Delga, N. Roblot, J. Lefevre, D. Job, J. Hazan, P.A. Curmi, J. Melki, Microtubule-targeting drugs rescue axonal swellings in cortical neurons from spastin knockout mice, Disease models & mechanisms, 6 (2013) 72-83.

[13] L. Qiang, W. Yu, M. Liu, J.M. Solowska, P.W. Baas, Basic fibroblast growth factor elicits formation of interstitial axonal branches via enhanced severing of microtubules, Molecular biology of the cell, 21 (2010) 334-344.

[14] R. Butler, J.D. Wood, J.A. Landers, V.T. Cunliffe, Genetic and chemical modulation of spastin-dependent axon outgrowth in zebrafish embryos indicates a role for impaired microtubule dynamics in hereditary spastic paraplegia, Disease models & mechanisms, 3 (2010) 743-751.

[15] J.H. Lumb, J.W. Connell, R. Allison, E. Reid, The AAA ATPase spastin links microtubule severing to membrane modelling, Biochimica et biophysica acta, 1823 (2012) 192-197.

[16] W. Yu, L. Qiang, J.M. Solowska, A. Karabay, S. Korulu, P.W. Baas, The microtubule-severing proteins spastin and katanin participate differently in the formation of axonal branches, Molecular biology of the cell, 19 (2008) 1485-1498.

[17] M.C. Stone, K. Rao, K.W. Gheres, S. Kim, J. Tao, C. La Rochelle, C.T. Folker, N.T. Sherwood, M.M. Rolls, Normal spastin gene dosage is specifically required for axon regeneration, Cell reports, 2 (2012) 1340-1350.

[18] N.T. Sherwood, Q. Sun, M. Xue, B. Zhang, K. Zinn, Drosophila spastin regulates synaptic microtubule networks and is required for normal motor function, PLoS biology, 2 (2004) e429.

[19] N. Trotta, G. Orso, M.G. Rossetto, A. Daga, K. Broadie, The hereditary spastic paraplegia gene, spastin, regulates microtubule stability to modulate synaptic structure and function, Current biology : CB, 14 (2004) 1135-1147.

[20] H.T. Tsang, T.L. Edwards, X. Wang, J.W. Connell, R.J. Davies, H.J. Durrington, C.J. O'Kane, J.P. Luzio, E. Reid, The hereditary spastic paraplegia proteins NIPA1, spastin and spartin are inhibitors of mammalian BMP signalling, Human molecular genetics, 18 (2009) 3805-3821.

[21] G. Orso, A. Martinuzzi, M.G. Rossetto, E. Sartori, M. Feany, A. Daga, Disease-related phenotypes in a Drosophila model of hereditary spastic paraplegia are ameliorated by treatment with vinblastine, The Journal of clinical investigation, 115 (2005) 3026-3034.

[22] K.R. Denton, L. Lei, J. Grenier, V. Rodionov, C. Blackstone, X.J. Li, Loss of spastin function results in disease-specific axonal defects in human pluripotent stem cell-based models of hereditary spastic paraplegia, Stem cells, 32 (2014) 414-423.

[23] Y. Song, S.T. Brady, Post-translational modifications of tubulin: pathways to functional diversity of microtubules, Trends Cell Biol, 25 (2015) 125-136.

[24] C. Janke, The tubulin code: molecular components, readout mechanisms, and functions, The Journal of cell biology, 206 (2014) 461-472.

[25] P.R. Kasher, K.J. De Vos, S.B. Wharton, C. Manser, E.J. Bennett, M. Bingley, J.D. Wood, R. Milner, C.J. McDermott, C.C. Miller, P.J. Shaw, A.J. Grierson, Direct evidence for axonal transport defects in a novel mouse model of mutant spastin-induced hereditary spastic paraplegia (HSP) and human HSP patients, Journal of neurochemistry, 110 (2009) 34-44.

[26] S. Havlicek, Z. Kohl, H.K. Mishra, I. Prots, E. Eberhardt, N. Denguir, H. Wend, S. Plotz, L. Boyer, M.C. Marchetto, S. Aigner, H. Sticht, T.W. Groemer, U. Hehr, A. Lampert, U. Schlotzer-Schrehardt, J. Winkler, F.H. Gage, B. Winner, Gene dosage-dependent rescue of HSP neurite defects in SPG4 patients' neurons, Human molecular genetics, (2014).

[27] A. Tarrade, C. Fassier, S. Courageot, D. Charvin, J. Vitte, L. Peris, A. Thorel, E. Mouisel, N. Fonknechten, N. Roblot, D. Seilhean, A. Dierich, J.J. Hauw, J. Melki, A mutation of spastin is responsible for swellings and impairment of transport in a region of axon characterized by changes in microtubule composition, Human molecular genetics, 15 (2006) 3544-3558.

[28] R. Jahn, R.H. Scheller, SNAREs - engines for membrane fusion, Nat Rev Mol Cell Biol, 7 (2006) 631-643.

[29] N.A. Ramakrishnan, M.J. Drescher, D.G. Drescher, The SNARE complex in neuronal and sensory cells, Molecular and cellular neurosciences, 50 (2012) 58-69.

[30] F. Daste, T. Galli, D. Tareste, Structure and function of longin SNAREs, Journal of cell science, 128 (2015) 4263-4272.

[31] J.I. Wojnacki Fonseca, T. Galli, Membrane traffic during axon development, Developmental neurobiology, (2016).

[32] S.L. Gupton, F.B. Gertler, Integrin signaling switches the cytoskeletal and exocytic machinery that drives neuritogenesis, Developmental cell, 18 (2010) 725-736.

[33] S. Martinez-Arca, P. Alberts, A. Zahraoui, D. Louvard, T. Galli, Role of tetanus neurotoxin insensitive vesicle-associated membrane protein (TI-VAMP) in vesicular transport mediating neurite outgrowth., The Journal of cell biology, 149 (2000) 889-899.

[34] S. Martinez-Arca, S. Coco, G. Mainguy, U. Schenk, P. Alberts, P. Bouille, M. Mezzina, A. Prochiantz, M. Matteoli, D. Louvard, T. Galli, A common exocytotic mechanism mediates axonal and dendritic outgrowth, J Neurosci, 21 (2001) 3830-3838.

[35] P. Alberts, R. Rudge, I. Hinners, A. Muzerelle, S. MartinezArca, T. Irinopoulou, V. Marthiens, S. Tooze, F. Rathjen, P. Gaspar, T. Galli, Cross talk between tetanus neurotoxin-insensitive vesicle- associated membrane protein-mediated transport and L1- mediated adhesion, Molecular biology of the cell, 14 (2003) 4207-4220.

[36] T. Cotrufo, F. Perez-Branguli, A. Muhaisen, O. Ros, R. Andres, T. Baeriswyl, G. Fuschini, T. Tarrago, M. Pascual, J. Urena, J. Blasi, E. Giralt, E.T. Stoeckli, E. Soriano, A signaling mechanism coupling netrin-1/deleted in colorectal cancer chemoattraction to SNARE-mediated exocytosis in axonal growth cones, J Neurosci, 31 (2011) 14463-14480.

[37] Z. Hua, S. Leal-Ortiz, S.M. Foss, C.L. Waites, C.C. Garner, S.M. Voglmaier, R.H. Edwards, v-SNARE composition distinguishes synaptic vesicle pools, Neuron, 71 (2011) 474-487.

[38] A. Scheuber, R. Rudge, L. Danglot, G. Raposo, T. Binz, J.C. Poncer, T. Galli, Loss of AP-3 function affects spontaneous and evoked release at hippocampal mossy fiber synapses, Proceedings of the National Academy of Sciences of the United States of America, 103 (2006) 16562-16567.

[39] L. Danglot, K. Zylbersztejn, M. Petkovic, M. Gauberti, H. Meziane, R. Combe, M.F. Champy, M.C. Birling, G. Pavlovic, J.C. Bizot, F. Trovero, F. Della Ragione, V. Proux-Gillardeaux, T. Sorg, D. Vivien, M. D'Esposito, T. Galli, Absence of TI-VAMP/Vamp7 leads to increased anxiety in mice, J Neurosci, 32 (2012) 1962-1968.

[40] A. Burgo, V. Proux-Gillardeaux, E. Sotirakis, P. Bun, A. Casano, A. Verraes, R.K. Liem, E. Formstecher, M. Coppey-Moisan, T. Galli, A molecular network for the transport of the TI-VAMP/VAMP7 vesicles from cell center to periphery, Developmental cell, 23 (2012) 166-180.

[41] E. Reid, M. Kloos, A. Ashley-Koch, L. Hughes, S. Bevan, I.K. Svenson, F.L. Graham, P.C. Gaskell, A. Dearlove, M.A. Pericak-Vance, D.C. Rubinsztein, D.A. Marchuk, A kinesin heavy chain (KIF5A) mutation in hereditary spastic paraplegia (SPG10), American journal of human genetics, 71 (2002) 1189-1194.

[42] M. Jouet, A. Rosenthal, G. Armstrong, J. MacFarlane, R. Stevenson, J. Paterson, A. Metzenberg, V. Ionasescu, K. Temple, S. Kenwrick, X-linked spastic paraplegia (SPG1), MASA syndrome and X-linked hydrocephalus result from mutations in the L1 gene, Nature genetics, 7 (1994) 402-407.

[43] K. Tsaneva-Atanasova, A. Burgo, T. Galli, D. Holcman, Quantifying neurite growth mediated by interactions among secretory vesicles, microtubules, and actin networks, Biophysical journal, 96 (2009) 840-857.

[44] A. Burgo, E. Sotirakis, M.C. Simmler, A. Verraes, C. Chamot, J.C. Simpson, L. Lanzetti, V. Proux-Gillardeaux, T. Galli, Role of Varp, a Rab21 exchange factor and TI-VAMP/VAMP7 partner, in neurite growth, EMBO reports, 10 (2009) 1117-1124.

[45] L. Danglot, A. Triller, A. Bessis, Association of gephyrin with synaptic and extrasynaptic GABAA receptors varies during development in cultured hippocampal neurons, Molecular and cellular neurosciences, 23 (2003) 264-278.

[46] J.P. Dompierre, J.D. Godin, B.C. Charrin, F.P. Cordelieres, S.J. King, S. Humbert, F. Saudou, Histone deacetylase 6 inhibition compensates for the transport deficit in Huntington's disease by increasing tubulin acetylation, J Neurosci, 27 (2007) 3571-3583.

[47] J.W. Hammond, C.F. Huang, S. Kaech, C. Jacobson, G. Banker, K.J. Verhey, Posttranslational modifications of tubulin and the polarized transport of kinesin-1 in neurons, Molecular biology of the cell, 21 (2010) 572-583.

[48] H. Witte, D. Neukirchen, F. Bradke, Microtubule stabilization specifies initial neuronal polarization, The Journal of cell biology, 180 (2008) 619-632.

[49] G. Abrahamsen, Y. Fan, N. Matigian, G. Wali, B. Bellette, R. Sutharsan, J. Raju, S.A. Wood, D. Veivers, C.M. Sue, A. Mackay-Sim, A patient-derived stem cell model of hereditary spastic paraplegia with SPAST mutations, Disease models & mechanisms, 6 (2013) 489-502.

[50] V. Daire, J. Giustiniani, I. Leroy-Gori, M. Quesnoit, S. Drevensek, A. Dimitrov, F. Perez, C. Pous, Kinesin-1 regulates microtubule dynamics via a c-Jun N-terminal kinase-dependent mechanism, The Journal of biological chemistry, 284 (2009) 31992-32001.

[51] D. Panda, H.P. Miller, A. Banerjee, R.F. Luduena, L. Wilson, Microtubule dynamics in vitro are regulated by the tubulin isotype composition, Proceedings of the National Academy of Sciences of the United States of America, 91 (1994) 11358-11362.

[52] N.A. Reed, D. Cai, T.L. Blasius, G.T. Jih, E. Meyhofer, J. Gaertig, K.J. Verhey, Microtubule acetylation promotes kinesin-1 binding and transport, Current biology : CB, 16 (2006) 2166-2172.

[53] D. Cai, D.P. McEwen, J.R. Martens, E. Meyhofer, K.J. Verhey, Single molecule imaging reveals differences in microtubule track selection between Kinesin motors, PLoS biology, 7 (2009) e1000216.

[54] J.D. Alper, F. Decker, B. Agana, J. Howard, The motility of axonemal dynein is regulated by the tubulin code, Biophysical journal, 107 (2014) 2872-2880.

[55] S. Coco, G. Raposo, S. Martinez, J.J. Fontaine, S. Takamori, A. Zahraoui, R. Jahn, M. Matteoli, D. Louvard, T. Galli, Subcellular localization of tetanus neurotoxin-insensitive vesicle-associated membrane protein (VAMP)/VAMP7 in neuronal cells: Evidence for a novel membrane compartment, J.Neurosci., 19 (1999) 9803-9812.

[56] A. Osen-Sand, J.K. Staple, E. Naldi, G. Schiavo, O. Rossetto, S. Petitpierre, A. Malgaroli, C. Montecucco, S. Catsicas, Common and distinct fusion proteins in axonal growth and transmitter release, J.Comp.Neurol., 367 (1996) 222-234.

[57] S. Schoch, F. Deak, A. Konigstorfer, M. Mozhayeva, Y. Sara, T.C. Sudhof, E.T. Kavalali, SNARE function analyzed in synaptobrevin/VAMP knockout mice, Science, 294 (2001) 1117-1122.

[58] T. Tojima, H. Akiyama, R. Itofusa, Y. Li, H. Katayama, A. Miyawaki, H. Kamiguchi, Attractive axon guidance involves asymmetric membrane transport and exocytosis in the growth cone, Nature neuroscience, 10 (2007) 58-66.

[59] J.S. Liu, C.R. Schubert, X. Fu, F.J. Fourniol, J.K. Jaiswal, A. Houdusse, C.M. Stultz, C.A. Moores, C.A. Walsh, Molecular basis for specific regulation of neuronal kinesin-3 motors by doublecortin family proteins, Mol Cell, 47 (2012) 707-721.

[60] V.K. Godena, N. Brookes-Hocking, A. Moller, G. Shaw, M. Oswald, R.M. Sancho, C.C. Miller, A.J. Whitworth, K.J. De Vos, Increasing microtubule acetylation rescues axonal transport and locomotor deficits caused by LRRK2 Roc-COR domain mutations, Nature communications, 5 (2014) 5245.

[61] D.D. Hurd, W.M. Saxton, Kinesin mutations cause motor neuron disease phenotypes by disrupting fast axonal transport in Drosophila, Genetics, 144 (1996) 1075-1085.

[62] M. Martin, S.J. Iyadurai, A. Gassman, J.G. Gindhart, Jr., T.S. Hays, W.M. Saxton, Cytoplasmic dynein, the dynactin complex, and kinesin are interdependent and essential for fast axonal transport, Molecular biology of the cell, 10 (1999) 3717-3728.

[63] G.B. Stokin, C. Lillo, T.L. Falzone, R.G. Brusch, E. Rockenstein, S.L. Mount, R. Raman, P. Davies, E. Masliah, D.S. Williams, L.S. Goldstein, Axonopathy and transport deficits early in the pathogenesis of Alzheimer's disease, Science, 307 (2005) 1282-1288.

[64] R.J. Vasquez, B. Howell, A.M. Yvon, P. Wadsworth, L. Cassimeris, Nanomolar concentrations of nocodazole alter microtubule dynamic instability in vivo and in vitro, Molecular biology of the cell, 8 (1997) 973-985.

[65] M.A. Jordan, Mechanism of action of antitumor drugs that interact with microtubules and tubulin, Current medicinal chemistry. Anti-cancer agents, 2 (2002) 1-17.

[66] M.A. Jordan, R.J. Toso, D. Thrower, L. Wilson, Mechanism of mitotic block and inhibition of cell proliferation by taxol at low concentrations, Proceedings of the National Academy of Sciences of the United States of America, 90 (1993) 9552-9556.

[67] G. Piperno, M. LeDizet, X.J. Chang, Microtubules containing acetylated alpha-tubulin in mammalian cells in culture, The Journal of cell biology, 104 (1987) 289-302.

[68] T. Stepanova, J. Slemmer, C.C. Hoogenraad, G. Lansbergen, B. Dortland, C.I. De Zeeuw, F. Grosveld, G. van Cappellen, A. Akhmanova, N. Galjart, Visualization of microtubule growth in cultured neurons via the use of EB3-GFP (end-binding protein 3-green fluorescent protein), J Neurosci, 23 (2003) 2655-2664.

[69] Y. Mimori-Kiyosue, N. Shiina, S. Tsukita, The dynamic behavior of the APC-binding protein EB1 on the distal ends of microtubules, Current biology : CB, 10 (2000) 865-868.

[70] O.A. Shemesh, M.E. Spira, Paclitaxel induces axonal microtubules polar reconfiguration and impaired organelle transport: implications for the pathogenesis of paclitaxel-induced polyneuropathy, Acta neuropathologica, 119 (2010) 235-248.

[71] C. Arregui, J. Busciglio, A. Caceres, H.S. Barra, Tyrosinated and detyrosinated microtubules in axonal processes of cerebellar macroneurons grown in culture, Journal of neuroscience research, 28 (1991) 171-181.

[72] F.J. Kull, R.D. Sloboda, A slow dance for microtubule acetylation, Cell, 157 (2014) 1255-1256.

[73] A. Szyk, A.M. Deaconescu, J. Spector, B. Goodman, M.L. Valenstein, N.E. Ziolkowska, V. Kormendi, N. Grigorieff, A. Roll-Mecak, Molecular basis for age-dependent microtubule acetylation by tubulin acetyltransferase, Cell, 157 (2014) 1405-1415.

[74] J.M. Solowska, G. Morfini, A. Falnikar, B.T. Himes, S.T. Brady, D. Huang, P.W. Baas, Quantitative and functional analyses of spastin in the nervous system: implications for hereditary spastic paraplegia, J Neurosci, 28 (2008) 2147-2157.

[75] H. Sudo, P.W. Baas, Acetylation of microtubules influences their sensitivity to severing by katanin in neurons and fibroblasts, J Neurosci, 30 (2010) 7215-7226.

[76] Y. Konishi, M. Setou, Tubulin tyrosination navigates the kinesin-1 motor domain to axons, Nature neuroscience, 12 (2009) 559-567.

[77] C. Zhao, J. Takita, Y. Tanaka, M. Setou, T. Nakagawa, S. Takeda, H.W. Yang, S. Terada, T. Nakata, Y. Takei, M. Saito, S. Tsuji, Y. Hayashi, N. Hirokawa, Charcot-Marie-Tooth Disease Type 2A Caused by Mutation in a Microtubule Motor KIF1Bβ Cell, 105 (2001) 587-597.

[78] P.D. Campbell, K. Shen, M.R. Sapio, T.D. Glenn, W.S. Talbot, F.L. Marlow, Unique function of Kinesin Kif5A in localization of mitochondria in axons, J Neurosci, 34 (2014) 14717-14732.

[79] M.H. Scheinfeld, R. Roncarati, P. Vito, P.A. Lopez, M. Abdallah, L. D'Adamio, Jun NH2-terminal kinase (JNK) interacting protein 1 (JIP1) binds the cytoplasmic domain of the Alzheimer's beta-amyloid precursor protein (APP), The Journal of biological chemistry, 277 (2002) 3767-3775.

[80] K.J. Verhey, D. Meyer, R. Deehan, J. Blenis, B.J. Schnapp, T.A. Rapoport, B. Margolis, Cargo of kinesin identified as JIP scaffolding proteins and associated signaling molecules, The Journal of cell biology, 152 (2001) 959-970.

[81] S.P. Gross, M. Vershinin, G.T. Shubeita, Cargo transport: two motors are sometimes better than one, Current biology : CB, 17 (2007) R478-486.

[82] R. Mallik, A.K. Rai, P. Barak, A. Rai, A. Kunwar, Teamwork in microtubule motors, Trends Cell Biol, 23 (2013) 575-582.

[83] S. Maday, A.E. Twelvetrees, A.J. Moughamian, E.L. Holzbaur, Axonal transport: cargo-specific mechanisms of motility and regulation, Neuron, 84 (2014) 292-309.

[84] W.J. Walter, V. Beranek, E. Fischermeier, S. Diez, Tubulin acetylation alone does not affect kinesin-1 velocity and run length in vitro, PloS one, 7 (2012) e42218.

[85] N. Kaul, V. Soppina, K.J. Verhey, Effects of alpha-tubulin K40 acetylation and detyrosination on kinesin-1 motility in a purified system, Biophysical journal, 106 (2014) 2636-2643.

[86] J. Atherton, A. Houdusse, C. Moores, MAPping out distribution routes for kinesin couriers, Biology of the cell / under the auspices of the European Cell Biology Organization, 105 (2013) 465-487.

[87] S. Millecamps, J.P. Julien, Axonal transport deficits and neurodegenerative diseases, Nature reviews, 14 (2013) 161-176.

[88] E. Chevalier-Larsen, E.L. Holzbaur, Axonal transport and neurodegenerative disease, Biochimica et biophysica acta, 1762 (2006) 1094-1108.

[89] K.R. Brunden, J.Q. Trojanowski, A.B. Smith, 3rd, V.M. Lee, C. Ballatore, Microtubule-stabilizing agents as potential therapeutics for neurodegenerative disease, Bioorganic & medicinal chemistry, 22 (2014) 5040-5049.

[90] P.W. Baas, F.J. Ahmad, Beyond taxol: microtubule-based treatment of disease and injury of the nervous system, Brain, 136 (2013) 2937-2951.

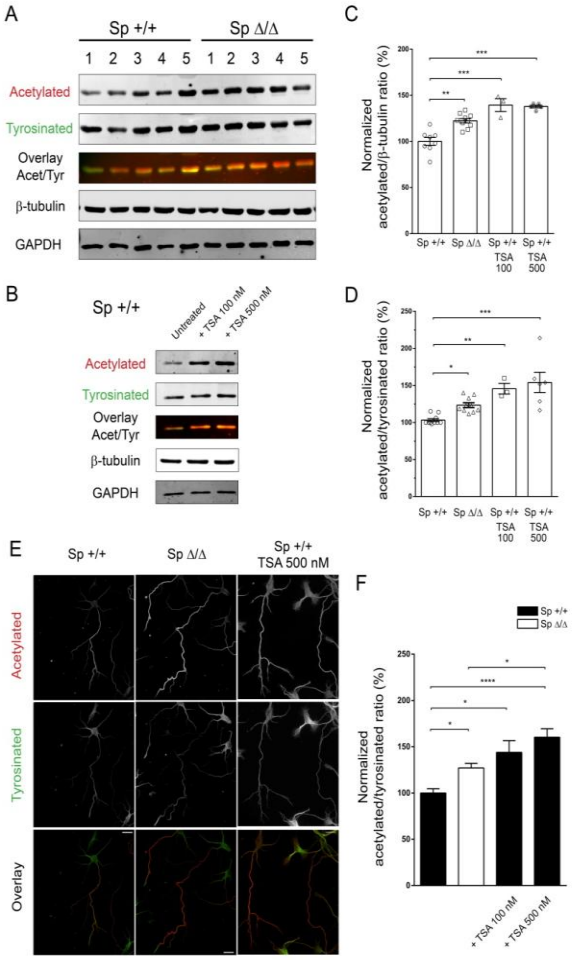

Figure 1

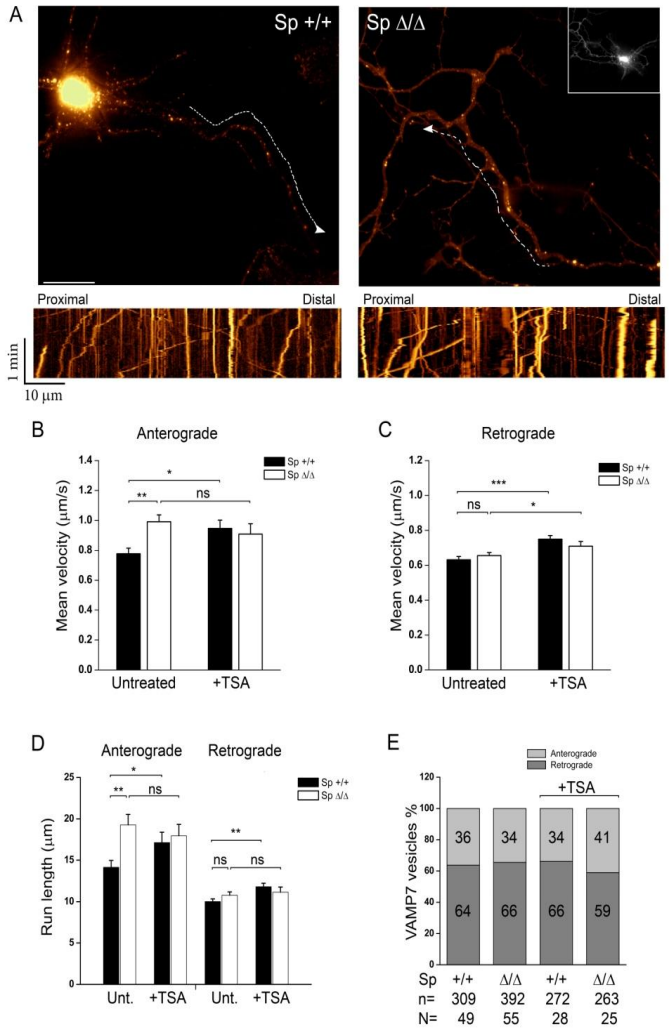

Figure 2

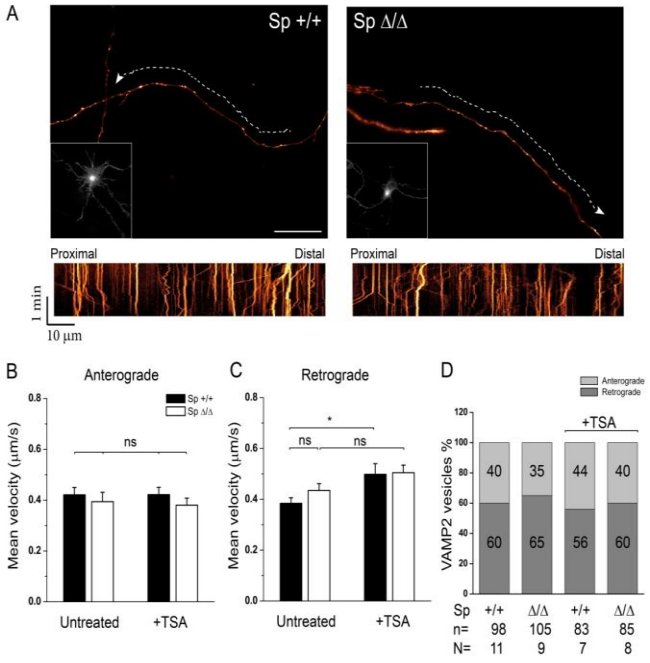

Figure 3

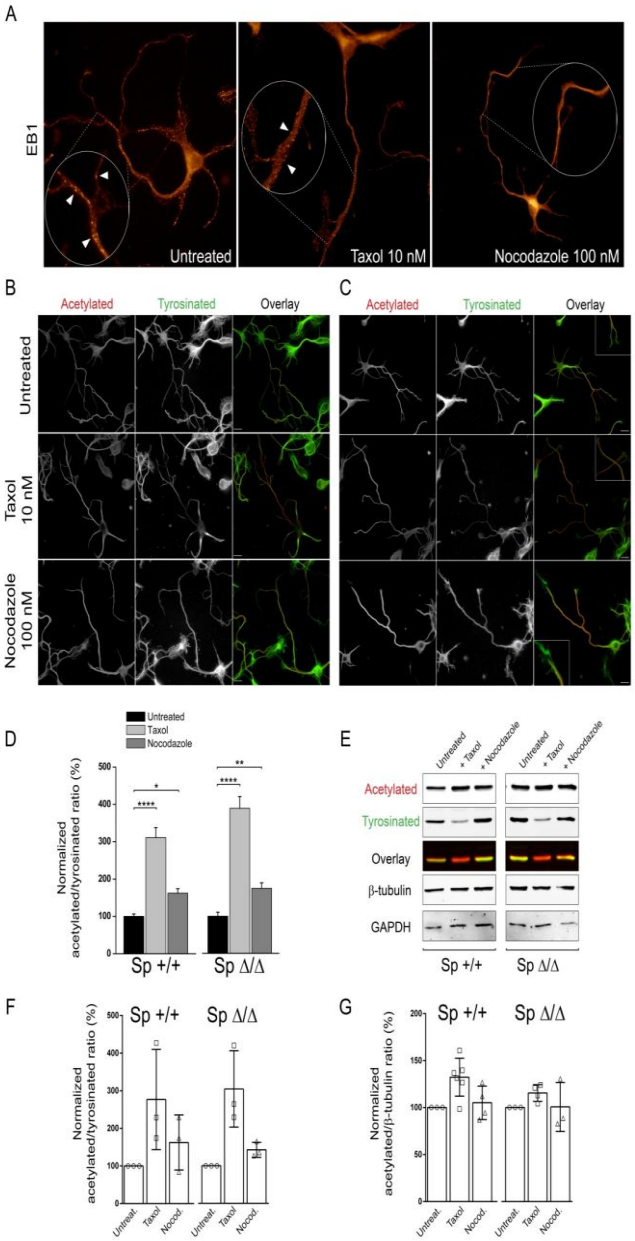
A
EB1
Untreated
Taxol 10 nM
Nocodazole 100 nM
B
C
Acetylated
Tyrosinated
Overlay
Untreated
Taxol 10 nM
Nocodazole 100 nM
D
Untreated
Taxol
Nocodazole
Normalized acetylated/tyrosinated ratio (%)
Sp +/+
Sp Δ/Δ
E
Untreated
+ Taxol
+ Nocodazole
Acetylated
Tyrosinated
Overlay
β-tubulin
GAPDH
Sp +/+
Sp Δ/Δ
F
Sp +/+
Sp Δ/Δ
Normalized acetylated/tyrosinated ratio (%)
Untreat.
Taxol
Nocod.
G
Sp +/+
Sp Δ/Δ
Normalized acetylated/β-tubulin ratio (%)
Untreat.
Taxol
Nocod.

Figure 4

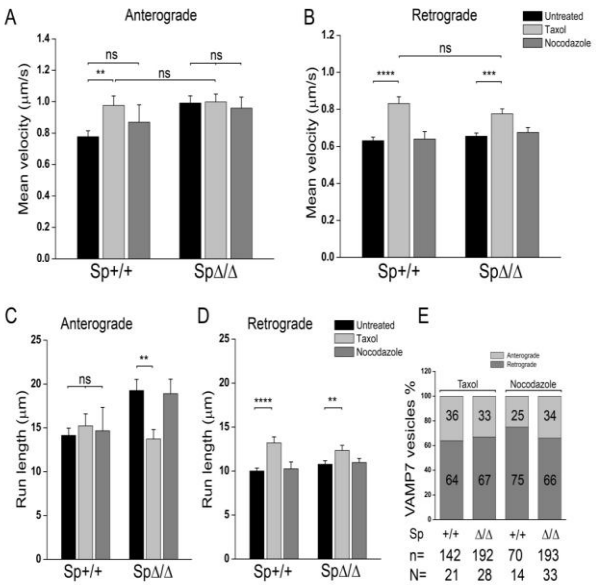

Figure 5

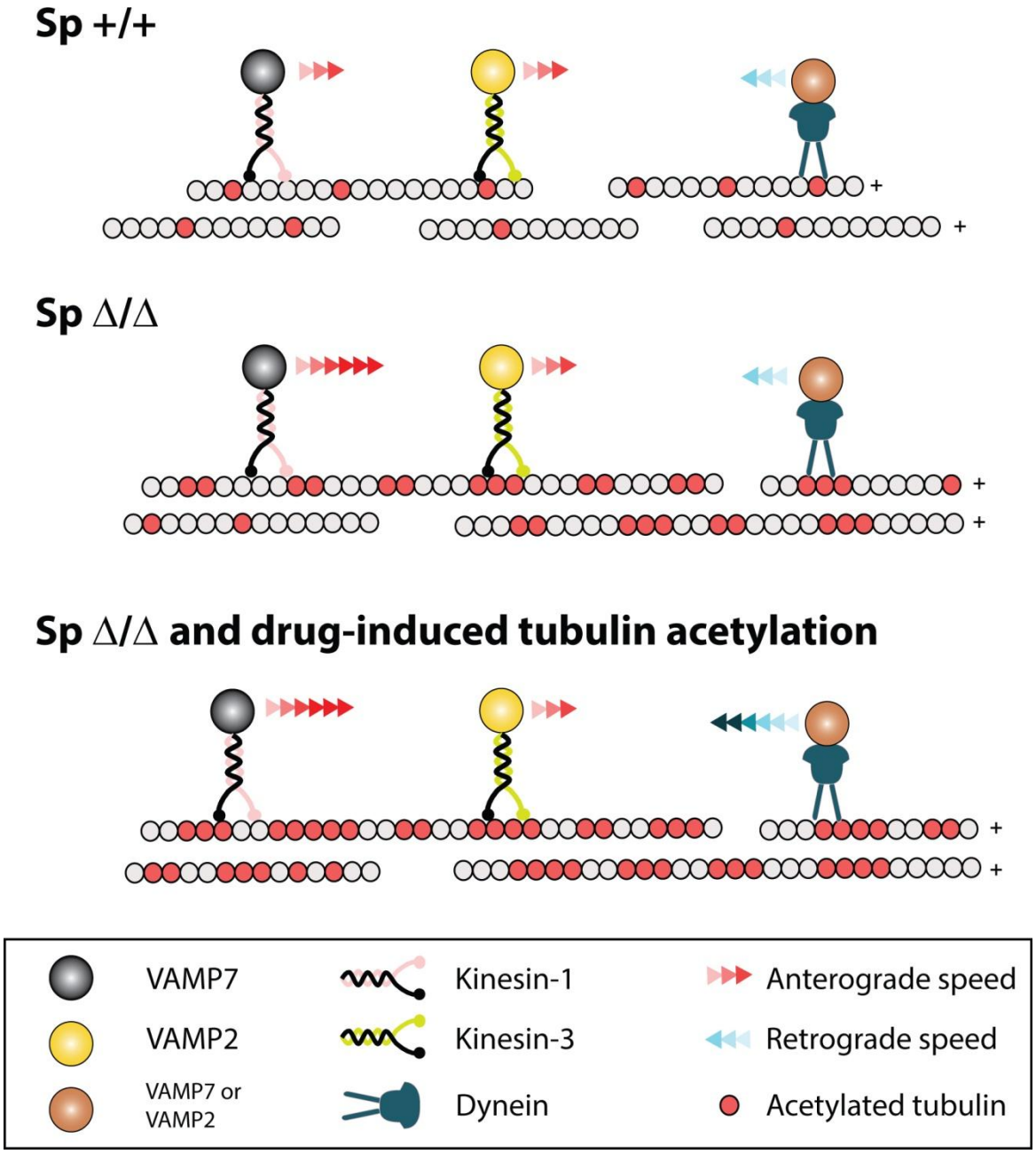

Figure 6

Table 1. VAMP7 mean velocities and run length.

Data are shown as mean ± SEM.

	VAMP7 mean velocity (μm/s)				VAMP7 mean run length (μm)			
	anterograde		retrograde		anterograde		retrograde	
	$Sp^{+/+}$	$Sp^{\Delta/\Delta}$	$Sp^{+/+}$	$Sp^{\Delta/\Delta}$	$Sp^{+/+}$	$Sp^{\Delta/\Delta}$	$Sp^{+/+}$	$Sp^{\Delta/\Delta}$
Untreated	0.77 ±0.04	0.99 ±0.04	0.63 ±0.02	0.65 ±0.02	14.2 ±0.8	19.3 ±1.3	10.0 ±0.3	10.8 ±0.4
TSA 500 nM	0.95 ±0.05	0.91 ±0.07	0.75 ±0.02	0.71 ±0.03	17.1 ±1.3	18.0 ±1.4	11.8 ±0.4	11.1 ±0.6
Taxol 10 nM	0.98 ±0.06	1.00 ±0.05	0.83 ±0.04	0.78 ±0.03	15.2 ±1.4	13.8 ±1.1	13.2 ±0.7	12.3 ±0.6
Nocodazole 100 nM	0.87 ±0.11	0.96 ±0.07	0.64 ±0.04	0.67 ±0.02	14.7 ±2.7	19.0 ±1.7	10.3 ±0.8	11.0 ±0.4

Highlights

- Acetylated tubulin is increased in SPG4-KO neurons.
- The anterograde speed of VAMP7 vesicles is enhanced in SPG4-KO neurons.
- Velocities of VAMP2 vesicles and mitochondria are not affected.
- Microtubule targeting agents did not rescue the altered VAMP7 traffic.
- Taxol increases the retrograde velocity of VAMP7 vesicles.